





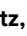







# A multi-channel x-ray temporal diagnostic for measurement of time-resolved electron temperature in cryogenic deuterium-tritium implosions at OMEGA

Cite as: Rev. Sci. Instrum. **92**, 023507 (2021); <https://doi.org/10.1063/5.0042329>

Submitted: 29 December 2020 . Accepted: 27 January 2021 . Published Online: 17 February 2021

 N. Kabadi,  A. Sorce,  C. Stoeckl,  H. W. Sio,  P. Adrian,  M. Bedzyk,  J. Frenje,  J. Katz, J. Knauer,  J. Percy, D. Weiner, B. A. Aguirre, R. Betti,  A. Birkel, D. Cao,  M. Gatu Johnson, D. Patel,  R. D. Petrasso, and S. P. Regan

## COLLECTIONS

Paper published as part of the special topic on [Proceedings of the 23rd Topical Conference on High-Temperature Plasma Diagnostics](#)



View Online



Export Citation



CrossMark

## ARTICLES YOU MAY BE INTERESTED IN

[Using millimeter-sized carbon-deuterium foils for high-precision deuterium-tritium neutron spectrum measurements in direct-drive inertial confinement fusion at the OMEGA laser facility](#)

Review of Scientific Instruments **92**, 023503 (2021); <https://doi.org/10.1063/5.0040549>

[An x-ray penumbral imager for measurements of electron-temperature profiles in inertial confinement fusion implosions at OMEGA](#)

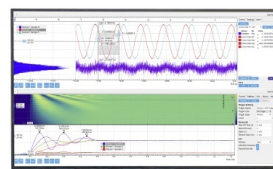
Review of Scientific Instruments **92**, 043548 (2021); <https://doi.org/10.1063/5.0041038>

[Absolute throughput calibration of multiple spherical crystals for the Orion High-REsolution X-ray spectrometer \(OHREX\)](#)

Review of Scientific Instruments **92**, 023509 (2021); <https://doi.org/10.1063/5.0043683>

Challenge us.

What are your needs for periodic signal detection?



Zurich  
Instruments

# A multi-channel x-ray temporal diagnostic for measurement of time-resolved electron temperature in cryogenic deuterium–tritium implosions at OMEGA

Cite as: Rev. Sci. Instrum. 92, 023507 (2021); doi: 10.1063/5.0042329

Submitted: 29 December 2020 • Accepted: 27 January 2021 •

Published Online: 17 February 2021



View Online



Export Citation



CrossMark

N. Kabadi,<sup>1,a)</sup> A. Sorce,<sup>2</sup> C. Stoeckl,<sup>2</sup> H. W. Sio,<sup>3</sup> P. Adrian,<sup>1</sup> M. Bedzyk,<sup>2</sup> J. Frenje,<sup>1</sup> J. Katz,<sup>2</sup> J. Knauer,<sup>2</sup> J. Percy,<sup>1</sup> D. Weiner,<sup>2</sup> B. A. Aguirre,<sup>4</sup> R. Betti,<sup>2</sup> A. Birkel,<sup>1</sup> D. Cao,<sup>2</sup> M. Gatu Johnson,<sup>1</sup> D. Patel,<sup>2</sup> R. D. Petrasso,<sup>1</sup> and S. P. Regan<sup>2</sup>

## AFFILIATIONS

<sup>1</sup>Massachusetts Institute of Technology Plasma Science and Fusion Center, Cambridge, Massachusetts 02139, USA

<sup>2</sup>University of Rochester Laboratory for Laser Energetics, Rochester, New York 14623, USA

<sup>3</sup>Lawrence Livermore National Laboratory, Livermore, California 94550, USA

<sup>4</sup>Sandia National Laboratories, Albuquerque, New Mexico 87123, USA

**Note:** Paper published as part of the Special Topic on Proceedings of the 23rd Topical Conference on High-Temperature Plasma Diagnostics.

<sup>a)</sup>Author to whom correspondence should be addressed: [kabadi@mit.edu](mailto:kabadi@mit.edu)

## ABSTRACT

Electron-temperature ( $T_e$ ) measurements in implosions provide valuable diagnostic information, as  $T_e$  is unaffected by residual flows and other non-thermal effects unlike ion temperature inferred from a fusion product spectrum. In OMEGA cryogenic implosions, measurement of  $T_e(t)$  can be used to investigate effects related to time-resolved hot-spot energy balance. The proposed diagnostic utilizes five fast-rise ( $\sim 15$  ps) scintillator channels with distinct x-ray filtering. Titanium and stepped aluminum filtering were chosen to maximize detector sensitivity in the 10 keV–20 keV range, as it has been shown that these x rays have similar density and temperature weighting to the emitted deuterium–tritium fusion neutrons. Initial data collected using a prototype nosecone on the existing neutron temporal diagnostic demonstrate the validity of this diagnostic technique. The proposed system will be capable of measuring spatially integrated  $T_e(t)$  with 20 ps time resolution and  $<10\%$  uncertainty at peak emission in cryogenic DT implosions.

Published under license by AIP Publishing. <https://doi.org/10.1063/5.0042329>

## I. BACKGROUND AND MOTIVATION

The goal of an inertial confinement fusion (ICF) experiment is to spherically compress deuterium and tritium (D and T) fuel to reach the high temperatures and densities necessary to achieve a burning plasma state. A DT fuel-shell is accelerated to high velocity. Shell kinetic energy is transferred to thermal energy of the central DT plasma (hot-spot), increasing the hot-spot density and temperature.<sup>1,2</sup> To reach ignition, this compression must happen symmetrically, efficiently transferring energy from the shell to the hot-spot. The details of this energy transfer and the overall

hot-spot energy balance must be understood to push toward fusion ignition.

Current understanding of hot-spot thermal energy relies heavily on ion temperatures inferred from the width of a fusion product spectrum, primarily from the DT-neutron and DD-neutron.<sup>3</sup> These measurements do provide valuable information but are not solely dependent on the hot-spot temperature as residual flows can substantially broaden the measured spectra and increase the apparent ion temperature.<sup>4–7</sup> In contrast, electron temperatures ( $T_e$ ) inferred from the shape of the emitted x-ray spectrum are unaffected by residual kinetic energy. For this reason, measured  $T_e$  can

provide valuable information about the thermal energy of the hot-spot, which will be used to investigate hot-spot energy balance, impacts of residual kinetic energy, ion–electron equilibration, and compression efficiency. In the cryo-DT implosions conducted at the OMEGA laser facility, the electrons and ions thermally equilibrate during peak compression.<sup>8</sup> This makes a spatially integrated time-resolved  $T_e$  measurement critical for understanding hot-spot energy balance.

The focus of this work is the design and initial testing of a fast-rise-scintillator-based diagnostic, which measures multiple x-ray emission histories at different energies at OMEGA. This diagnostic will be referred to as the Cryo Particle X-ray Temporal Diagnostic (CryoPXTD) as it is a new upgraded version of the existing Particle X-ray Temporal Diagnostic (PXTD)<sup>9</sup> with better temporal resolution and shielding to allow the use on high-yield cryo-DT implosions. This paper will focus on x-ray measurement, but the system will also be capable of measuring fusion product emission histories. The measured x-ray emission histories are used to infer the time-resolved electron temperature [ $T_e(t)$ ] with 20 ps time resolution and 10% uncertainty at peak emission. The subsequent sections discuss diagnostic requirements for achieving these goals, as well as initial tests using a prototype design that is based on the existing neutron temporal diagnostic (NTD) infrastructure.<sup>10</sup>

## II. DIAGNOSTIC DESIGN

A synthetic diagnostic was used to simulate streak images similar to real data. The relative signal level in the different channels was computed using tabulated transmission as a function of photon energy for filters and energy absorption for the scintillator material.<sup>11</sup> A LILAC<sup>12</sup> hydrodynamic simulation of OMEGA Cryo implosion 84646 was post processed with SPECT3D<sup>13</sup> to compute the total time-resolved x-ray emission spectrum. This was fed into the synthetic diagnostic to produce a streak image, and the input spectrum was scaled so that the synthetic signal level was consistent with data collected with a prototype system. Realistic noise caused by fusion DT-neutron (DTn) directly impacting the streak camera was sampled directly from the background of NTD. The synthetic data were analyzed by first taking line-outs to produce measured time histories. Then, the data are binned on the 20 ps time scale, and the simulated impulse response function is deconvolved from each channel. This results in multiple x-ray emission histories. The histories in each time bin are fit to an exponential bremsstrahlung spectrum to infer  $T_e(t)$  using tabulated transmission and absorption properties. Inferring  $T_e(t)$  using differential x-ray filtering is the technique employed by the existing PXTD<sup>9</sup> and hard x-ray detector<sup>14</sup> on OMEGA. Differential filtering was chosen over crystal-based measurements, such as NIF's continuum x-ray spectrometer,<sup>15</sup> for increased signal statistics and the flexibility to measure different x-ray energy ranges and fusion products with a simple filter change.

### A. Channel and filter selection

#### 1. Number of channels

The system utilizes multiple scintillator channels within a 20 mm diameter cross section positioned 90 mm from the target

chamber center (TCC) to measure the shape of the emitted x-ray spectrum. Increasing the number of channels provides more information about the spectral shape and decreases the impact of random errors in the filter calibrations. Including too many channels decreases the photon statistics in each channel and therefore increases the statistical uncertainty of the  $T_e$  measurement. The number of channels should be selected to minimize the uncertainty in the inferred  $T_e$ . The synthetic diagnostic was used to simulate the impact of the realistic signal to noise ratio, photon statistics,<sup>16</sup> and filter thickness calibration uncertainty of 0.5  $\mu\text{m}$ . The system uncertainty at peak x-ray emission with three to eight scintillator channels was calculated. Based on these calculations, five channels are selected as they provide 8% uncertainty and are robust to calibration errors. This design requires that the optical relay images the 20 mm scintillator array with 0.4 mm spatial resolution.

#### 2. Filter material and thickness

To infer  $T_e$ , each of the five channels must have a different filter thickness and/or a material to be sensitive to different x-ray energies. The CryoPXTD is designed to measure x rays in the 10 keV–20 keV range. This range is selected for the x-ray measurement to be weighted to similar regions as the DTn allows direct comparison to nuclear observables.<sup>8</sup> Through optimization with the synthetic diagnostic, it was found that a 100  $\mu\text{m}$  thick Ti filter in combination with stepped Al filters 100  $\mu\text{m}$ , 200  $\mu\text{m}$ , 300  $\mu\text{m}$ , 400  $\mu\text{m}$ , and 500  $\mu\text{m}$  thick meets the energy-range requirement while preserving the high photon statistics necessary to achieve <10% uncertainty at peak emission. The physical height of each scintillator channel is varied to equalize the total statistics across all channels. The final front end design is shown in Fig. 1. The simulated relative efficiencies of these five channels are shown in Fig. 2(a), and the expected signal vs energy for a  $T_e = 3$  keV bremsstrahlung spectrum is shown in Fig. 2(b). At  $T_e = 3$  keV, >90% of the signal amplitude from all the five channels comes from x rays in the 10 keV–20 keV range. The actual efficiencies have been measured using a filter characterization test bench to minimize uncertainty.<sup>17</sup>

### B. Temporal response

At the onset of the compression phase in OMEGA cryo implosions, the ions are expected to have a higher temperature than the electrons, as ions are preferentially heated during the preceding shock phase. By peak emission time, the ion and electron temperatures are expected to have equilibrated to within  $\sim 10\%$ .<sup>8</sup> As the electrons and ions do not start out in thermal equilibrium, a time-resolved measurement within  $\sim 6$  independent bins is necessary to properly constrain the hot-spot energy balance. As the x-ray emission histories are expected to be  $\sim 70$  ps FWHM, 20 ps temporal resolution is required. With this resolution, the thermal energy content of the hot-spot as a function of time will be constrained.

Commercially available 1-mm thick BC-422 fast-rise scintillators were selected because they have been demonstrated to achieve rise times <20 ps.<sup>18</sup> For this paper, the rise time is taken to be  $\sim 15$  ps although more accurate measurement of the rise would increase the accuracy of the time resolution estimates. Given that BC-422 scintillators have a slow decaying tail with  $\sim 1.2$  ns fall time, all of the information is encoded in the rising edge and a deconvolution approach must be used to recover the emission history. The light emission

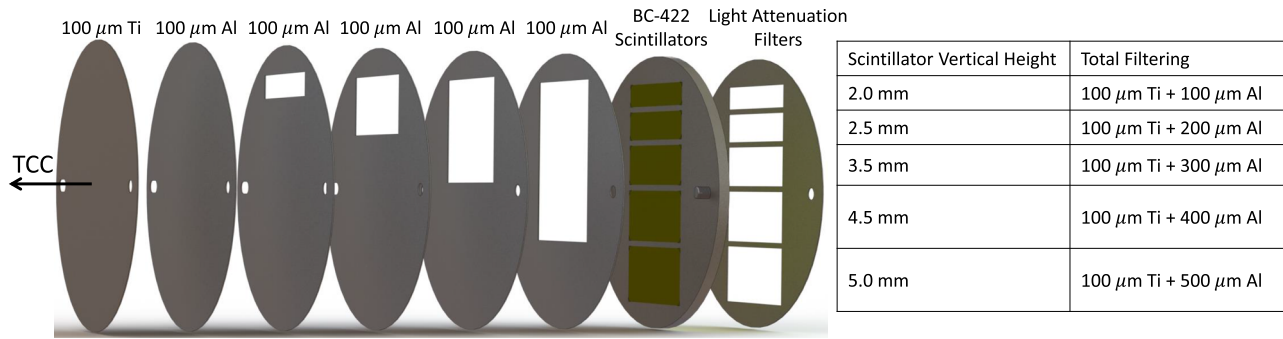


**FIG. 1.** An exploded view of the final filtering and scintillator design for the CryoPXTD. The scintillators will all be 1 mm thick. A bracket for scintillator light attenuation filters is included, but for this design none are used. The scintillator light will be relayed to a shielded streak camera as shown in Fig. 3.

from the scintillators is transported through an optical relay to a streak camera. This camera must be in a location that is shielded from the emitted DTn to reduce the impact of direct neutron incidence background. The effective temporal resolution of the entire system will be impacted by the scintillator rise time, chromatic dispersion in the optical relay, and response of the streak tube and camera.

As was investigated by Lerche *et al.*,<sup>19</sup> the minimum temporal dispersion of the P510 tube-camera is ~10 ps. Electron-optics simulations of the Photek DS tube to be used for this diagnostic show similar temporal broadening. Chromatic temporal dispersion

results as different wavelength photons from the scintillator emission spectrum take different times to traverse the optical relay. A preliminary mechanical and optical design has been completed as shown in Fig. 3. This design meets the spatial resolution requirement of 0.4 mm. The FWHM of the temporal spread resulting from transporting the full scintillator spectrum through the relay is estimated to be 20 ps. In combination with the 15 ps scintillator rise, this is above the design requirement. By using a narrow band-pass filter ( $\Delta\lambda \sim 20$  nm) situated in front of the streak camera, chromatic temporal dispersion can be reduced to 8 ps FWHM at the cost of ~1/2 of the signal photons. Assuming Gaussian broadening, the FWHM of the total system temporal dispersion is given by  $\sqrt{15^2 + 10^2 + 20^2} ps \approx 27 ps$ . Including the band-pass filter, the total dispersion is reduced to  $\sqrt{15^2 + 10^2 + 8^2} ps \approx 20 ps$ , satisfying the physics requirement. All previous and subsequent design work includes this bandpass filter reducing the signal level by 1/2.

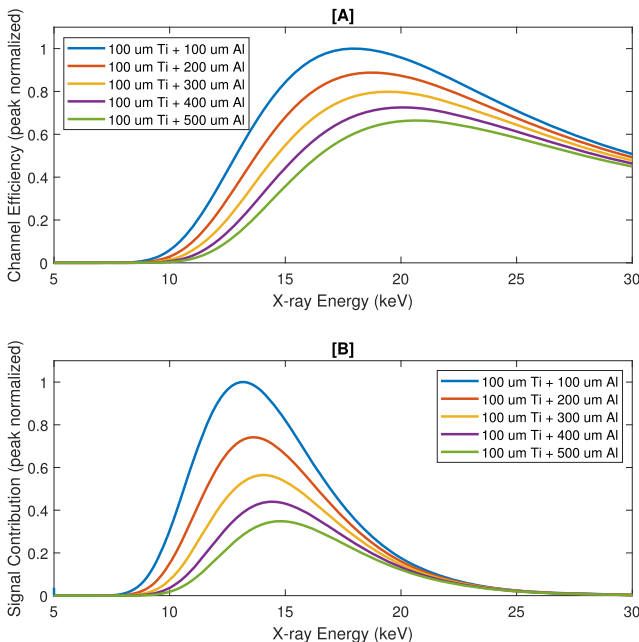


**FIG. 2.** (a) Peak normalized efficiency curves vs x-ray energy for each channel, estimated as the total x-ray energy absorption in the scintillator behind each filter stack. (b) The expected relative contribution to the signals vs x-ray energy for a  $T_e = 3$  keV bremsstrahlung spectrum.

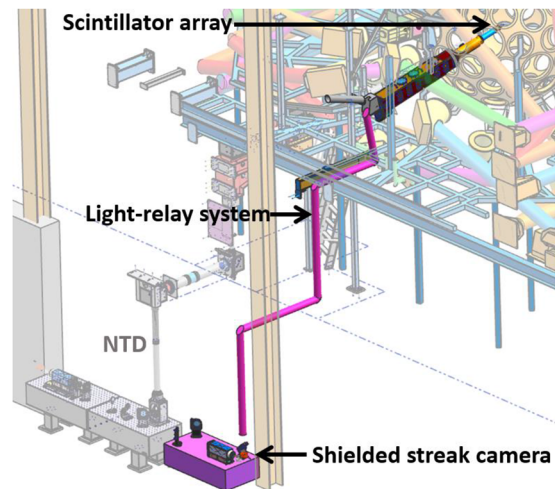


**FIG. 3.** Preliminary engineering design of the CryoPXTD diagnostic on the OMEGA target chamber with a light relay transporting the signal to a shielded streak camera. The NTD can be seen in the background using a similar relay-camera system.



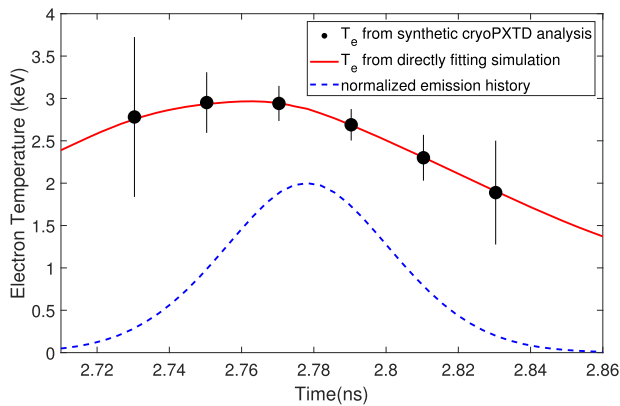


**FIG. 4.** Black points show  $T_e(t)$  inferred from synthetic CryoPXTD data generated for shot 84646. The solid red curve shows the result from directly fitting the simulated x-ray spectrum in the 10 keV–20 keV range. The simulated x-ray emission history shape is shown in blue dashed line for reference.

### C. Final design

The final proposed front-end design is shown in Fig. 1. The results of generating synthetic CryoPXTD data and then analyzing the data for  $T_e(t)$  are shown in Fig. 4. Analysis of the synthetic CryoPXTD data shows excellent agreement with the  $T_e(t)$  inferred from directly fitting the simulated x-ray spectrum in the 10 keV–20 keV range. The error bars on the synthetic analysis are a combination of statistical,<sup>16</sup> calibration, and signal to noise contributions. Based on the previously discussed calculations, the dominant source of uncertainty at peak emission is noise. Work is underway at LLE to increase shielding around the area that the camera will be located. This will reduce the  $T_e$  uncertainty at peak emission to below 5%.

### III. PROTOTYPE TESTING

A prototype system was tested using a four-channel nosecone and the existing NTD infrastructure.<sup>10</sup> Similar to the design outlined here, NTD uses a BC-422 scintillator coupled to a shielded streak camera via an optical relay. A portion of the NTD relay and the camera can be seen in Fig. 3. The prototype used a 100  $\mu\text{m}$  Ti filter and Al filters 300  $\mu\text{m}$ , 400  $\mu\text{m}$ , and 500  $\mu\text{m}$  thick. The fourth channel was dedicated to measure the DTn emission history with 1 mm of tungsten. The DTn signal from cryo implosions is 20 times higher amplitude than the core x-ray emission in the 10 keV–20 keV energy range. As the diagnostic settings are driven by the primary DTn emission history measurement, the x-ray signals have poor statistics. In a dedicated system, signal statistics will be greatly improved.

Data collected on OMEGA Cryo-DT shot 98768 are shown in Fig. 5. Figure 5(a) shows the raw streak image, and Fig. 5(b) shows line-outs from the streak image for each of the four channels zoomed in on the x-ray component. The resulting x-ray emission history is shown in Fig. 5(c). The fast rise of the scintillator emission and, therefore, the peak of the x-ray emission history are well correlated with the time of peak nuclear production, or DTn bang time. The results of this test validate the proposed diagnostic technique

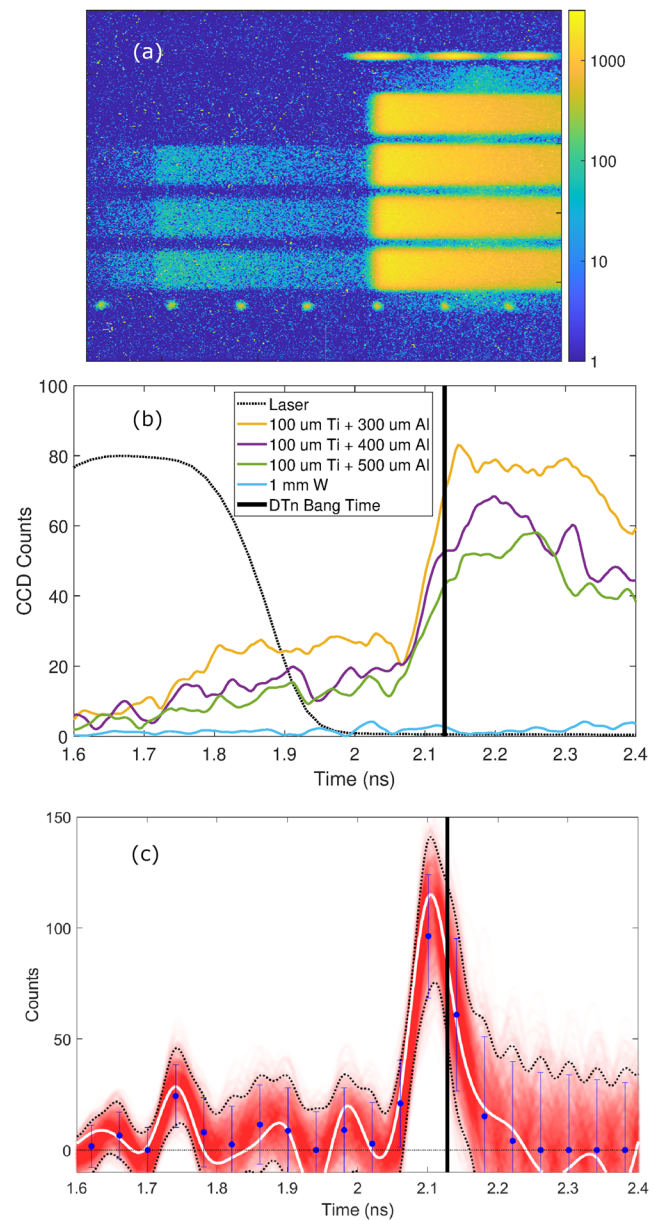


**FIG. 5.** (a) Streak image collected on OMEGA Cryo-DT implosion 98768 using a four-channel design and the NTD infrastructure. (b) Signals shown in (a) zoomed in on the x-ray component. The end of the laser pulse is included as a black dashed curve, and the DTn bang time is indicated by the black vertical line. (c) The result of deconvolving the impulse response from the sum of the line-outs in (b).

and verify that, in a dedicated diagnostic, the measured signals will have sufficient statistics to infer  $T_e(t)$  as this absolute signal level was used in the previous design section.

Additional testing was done on room-temperature shock-driven implosions. For these implosions, the x-ray emission levels were much higher allowing simultaneous measurement of the DTn and x-ray emission histories with good statistics. The raw streak

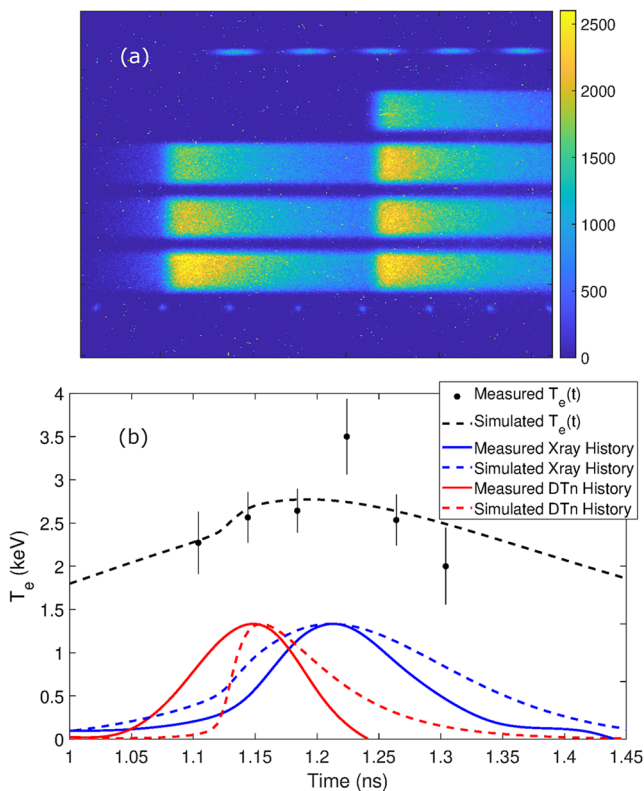


**FIG. 6.** (a) Raw streak image collected on OMEGA shock driven DT-filled implosion 98811. (b) The result of analyzing the data shown in Fig. 6(a) for  $T_e(t)$  is shown as black points. The deconvolved x-ray and DTn emission histories are shown as solid curves.  $T_e(t)$ , x-ray emission, and DTn emission histories from a HYADES hydrodynamic simulation are shown as dashed curves.

image is shown in Fig. 6(a). From these high quality x-ray emission histories,  $T_e(t)$  is inferred on the 40 ps time scale. The inferred  $T_e(t)$  as well as the total x-ray emission and DTn emission histories are shown in Fig. 6(b). The results of a hydrodynamic HYADES simulation are also shown for reference. The simulated  $T_e(t)$  shows good agreement with the measurement. While the exact shapes of the DTn and x-ray emission histories are not identical, the simulation reproduces the measured 65 ps between the x ray and DTn bang time.

On half of the prototype cryo measurements, an early time signal of  $20\times$  higher amplitude is present. Due to its intermittent nature, the source of this signal is likely not the implosion but rather a diagnostic or hardware effect that needs to be identified and mitigated. On warm implosions, this signal was never present indicating that it may be related to the cryo-specific hardware.

#### IV. CONCLUSIONS

Proof-of-principle tests of the CryoPXTD concept have been experimentally executed. Construction of the CryoPXTD diagnostic as outlined in this paper would allow measurement of  $T_e(t)$  with 20 ps time resolution and  $<10\%$  uncertainty at peak

emission on OMEGA cryo implosions. Other filter configurations can be designed for different implosion types and as LLE continues to improve cryo implosion performance. Plans already exist to use this diagnostic for precision measurement of multiple nuclear emission histories on NLUF experiments.

#### ACKNOWLEDGMENTS

This material is based upon work supported by the Department of Energy, National Nuclear Security Administration under Award Nos. DE-NA0003868 and DE-NA0003938.

This report was prepared as an account of work sponsored by an agency of the United States Government. Neither the United States Government nor any agency thereof, nor any of their employees, makes any warranty, express or implied, or assumes any legal liability or responsibility for the accuracy, completeness, or usefulness of any information, apparatus, product, or process disclosed, or represents that its use would not infringe privately owned rights. Reference herein to any specific commercial product, process, or service by trade name, trademark, manufacturer, or otherwise does not necessarily constitute or imply its endorsement, recommendation, or favoring by the United States Government or any agency thereof. The views and opinions of authors expressed therein do not necessarily state or reflect those of the United States Government or any agency thereof.

#### DATA AVAILABILITY

The data that support the findings of this study are available from the corresponding author upon reasonable request.

#### REFERENCES

- R. S. Craxton, K. S. Anderson, T. R. Boehly, V. N. Goncharov, D. R. Harding, J. P. Knauer, R. L. McCrory, P. W. McKenty, D. D. Meyerhofer, J. F. Myatt, A. J. Schmitt, J. D. Sethian, R. W. Short, S. Skupsky, W. Theobald, W. L. Kruer, K. Tanaka, R. Betti, T. J. B. Collins, J. A. Delettrez, S. X. Hu, J. A. Marozas, A. V. Maximov, D. T. Michel, P. B. Radha, S. P. Regan, T. C. Sangster, W. Seka, A. A. Solodov, J. M. Soures, C. Stoeckl, and J. D. Zuegel, *Phys. Plasmas* **22**, 110501 (2015).
- J. D. Lindl, P. Amendt, R. L. Berger, S. G. Glendinning, S. H. Glenzer, S. W. Haan, R. L. Kauffman, O. L. Landen, and L. J. Suter, *Phys. Plasmas* **11**(2), 339 (2004).
- V. Y. Glebov, C. Stoeckl, T. C. Sangster, S. Roberts, G. J. Schmid, R. A. Lerche, and M. J. Moran, *Rev. Sci. Instrum.* **75**, 3559 (2004).
- T. J. Murphy, *Phys. Plasmas* **21**(7), 072701 (2014).
- M. Gatu Johnson, B. D. Appelbe, J. P. Chittenden, A. Crilly, J. Delettrez, C. Forrest, J. A. Frenje, V. Y. Glebov, W. Grimble, B. M. Haines, I. V. Igumenshchev, R. Janezic, J. P. Knauer, B. Lahmann, F. J. Marshall, T. Michel, F. H. Séguin, C. Stoeckl, C. Walsh, A. B. Zylstra, and R. D. Petrasso, *Phys. Plasmas* **26**(1), 012706 (2019).
- K. M. Woo, R. Betti, O. M. Mannion, C. J. Forrest, J. P. Knauer, V. N. Goncharov, P. B. Radha, D. Patel, V. Gopalaswamy, and V. Y. Glebov, *Phys. Plasmas* **27**, 062702 (2020).
- O. M. Mannion, A. J. Crilly, J. Frenje, V. Y. Glebov, M. G. Johnson, J. P. Knauer, Z. L. Mohamed, S. P. Regan, H. G. Rinderknecht, M. H. Romanofsky, C. Stoeckl, W. Theobald, and K. M. Woo, in 23rd Topical Conference on High Temperature Plasma Diagnostics, 2020.
- D. Cao, R. C. Shah, S. P. Regan, R. Epstein, I. V. Igumenshchev, V. Gopalaswamy, A. R. Christopherson, W. Theobald, P. B. Radha, and V. N. Goncharov, *Phys. Plasmas* **26**, 082709 (2019).
- H. Sio, J. A. Frenje, J. Katz, C. Stoeckl, D. Weiner, M. Bedzyk, V. Glebov, C. Sorce, M. Gatu Johnson, H. G. Rinderknecht, A. B. Zylstra, T. C. Sangster, S. P. Regan,

- T. Kwan, A. Le, A. N. Simakov, W. T. Taitano, L. Chacòn, B. Keenan, R. Shah, G. Sutcliffe, and R. D. Petrasso, *Rev. Sci. Instrum.* **87**, 11D701 (2016).
- <sup>10</sup>C. Stoeckl, R. Boni, F. Ehrne, C. J. Forrest, V. Y. Glebov, J. Katz, D. J. Lonobile, J. Magoon, S. P. Regan, M. J. Shoup, A. Sorce, C. Sorce, T. C. Sangster, and D. Weiner, *Rev. Sci. Instrum.* **87**, 053501 (2016).
- <sup>11</sup>[curtis.suplee@nist.gov](mailto:curtis.suplee@nist.gov), “X-ray mass attenuation coefficients” (2009), last modified 11 December 2019 T10:11-05:00.
- <sup>12</sup>J. Delettrez, R. Epstein, M. C. Richardson, P. A. Jaanimagi, and B. L. Henke, *Phys. Rev. A* **36**, 3926 (1987).
- <sup>13</sup>J. MacFarlane, I. Golovkin, P. Wang, P. Woodruff, and N. Pereyra, *High Energy Density Phys.* **3**, 181 (2007).
- <sup>14</sup>C. Stoeckl, V. Y. Glebov, D. D. Meyerhofer, W. Seka, B. Yaakobi, R. P. J. Town, and J. D. Zuegel, *Rev. Sci. Instrum.* **72**, 1197 (2001).
- <sup>15</sup>D. B. Thorn, A. MacPhee, J. Ayers, J. Galbraith, C. M. Hardy, N. Izumi, D. K. Bradley, L. A. Pickworth, B. Bachmann, B. Koziowski, O. Landen, D. Clark, M. B. Schneider, K. W. Hill, M. Bitter, S. Nagel, P. M. Bell, S. Person, H. Y. Khater, C. Smith, and J. Kilkenny, “Target diagnostics physics and engineering for inertial confinement fusion VI,” *Proc. SPIE* **10390**, 1039009 (2017).
- <sup>16</sup>R. A. Lerche and T. J. Ognibene, *Rev. Sci. Instrum.* **70**, 1217 (1999).
- <sup>17</sup>J. Percy, N. Kabadi, A. Birkel, P. Adrian, B. Lahmann, B. Reichelt, T. M. Johnson, G. Sutcliffe, J. Kunimune, M. Gatu-Johnson, A. Bose, R. Petrasso, and C. K. Li, “Characterizing x-ray transmission through filters used in HEDP diagnostics,” *Rev. Sci. Instrum.* (unpublished).
- <sup>18</sup>R. A. Lerche and D. W. Phillon, in *Conference Record of the 1991 IEEE Nuclear Science Symposium and Medical Imaging Conference* (IEEE, 1991), Vol. 1, pp. 167–170.
- <sup>19</sup>R. A. Lerche, J. W. McDonald, R. L. Griffith, G. Vergel de Dios, D. S. Andrews, A. W. Huey, P. M. Bell, O. L. Landen, P. A. Jaanimagi, and R. Bon, “Preliminary performance measurements for a streak camera with a large-format direct-coupled charge-coupled device readout,” *Rev. Sci. Instrum.* **75**, 4042 (2004).